RSC Advances

ROYAL SOCIETY OF CHEMISTRY

www.rsc.org/advances

Supercapacitor Characteristics of Pressurized RuO_2/Carbon Powder as Binder-Free Electrodes

Seung-Chul Hong[a], Sanghoon Kim[b], Woo-Jin Jang[a], Tai-Hoon Han[a], Jung-Pyo Hong[a], Joon-Suk Oh[a], Taeseon Hwang[a], Youngkwan Lee[c], Jun-Ho Lee[b,*], Jae-Do Nam[a,b,**],

[a]Department of Polymer Science and Engineering, Sungkyunkwan University, 300 Chunchun-dong, Jangan-gu, Suwon, Gyeonggi-do 440-746, Republic of Korea

[b]Department of Energy Science, Sungkyunkwan University, 300 Chunchun-dong, Jangan-gu, Suwon, Gyeonggi-do 440-746, Republic of Korea

[c]Department of Chemical Engineering, Sungkyunkwan University, 300 Chunchun-dong, Jangan-gu, Suwon, Gyeonggi-do 440-746, Republic of Korea

*, ** Corresponding authors: Jun-Ho Lee, Jae-Do Nam,

Email: neodraft@skku.edu, jdnam@skku.edu

Phone: +82-31-290-7285

Fax: +82-31-292-8790

KEYWORDS: supercapacitor; pseudocapacitor; RuO_2; hybrid capacitor; binder-free

Abstract

RuO_2/carbon powder electrodes have been designed to be enclosed in a supercapacitor cell and compressed under a constant pressure (4.84 $kg_f cm^{-2}$), which could overcome the binder failure under the repeated volumetric changes. In this binder-free powder electrode system, the resistance and ESR are substantially decreased (0.39 Ωat 1 kHz) and the capacitive retention is also greatly improved (7% decrement after 4,000 cycles) with a maximum specific capacitance of 835 F (g of total electrode weight)$^{-1}$, corresponding to 1391.7 F (g of RuO_2 weight)$^{-1}$, which is likely close to the intrinsic energy-storage capability of RuO_2 materials. Comparing the specific capacitances at different discharge rates of 5 mV s^{-1} and 100 mV s^{-1}, a decrement of only 24% occurs in specific capacitance, which is considered to be excellent in RuO_2 systems. Furthermore, in the Ragone plot analysis, the developed binder-free system shows an excellent energy and power density of 24.9 Wh kg^{-1} and 16.1 kW kg^{-1}, respectively, at 50 mV s^{-1}, which are ca. 63.2% and 44.7% higher, respectively, than those of a typical binder-containing system (11.1 Wh kg^{-1} and 7.2 kW kg^{-1}).

Introduction

As important energy storage devices, electrochemical supercapacitors have unique characteristics of rapid charge/discharge speed, long life cycle, and high power density [1]. However, the energy density of the supercapacitor is considered low compared to rechargeable batteries; e.g., 5~20 Wh kg^{-1} for commercialized electric double-layer supercapacitors (EDLC) and ~170 $Whkg^{-1}$ for Li-ion batteries [2-3]. Pseudocapacitors, as an intermediate system between dielectric capacitors and batteries, have attracted much interest due to their high power density and higher energy density [4,5]. Pseudocapacitors normally combine non-faradic electrostatic charge storage with Faradaic redox reactions, and they often give much higher capacitances than EDLCs [6,7].

Many transition metal oxides have shown promising pseudocapacitance stemming from the pseudo-capacitance via reversible redox reaction with hydrogen ions [8-10]. Among transition metal oxides, for example, MnO_2, NiO, and V_2O_5 have received considerable attention due to their high theoretical specific capacitance, large surface area, low cost, and non-polluting properties [11]. On the other hand, these metal oxides have poor electrical conductivity, resulting in reduced capacitive performance and slow electron transport at high electrical rates, limiting their practical application [12]. In particular, RuO_2 is a typical material for pseudocapacitors due to its remarkably high theoretical specific capacitance (1358 F g^{-1}) and exceptional properties such as metallic-type conductivity, wide potential window, and highly reversible redox reaction [13,14]. The optimization of the pseudocapacitance of RuO_2 has been reported as 720 F g^{-1} in hydrous form [15], 800 Fg^{-1} in meso-porous hydrous thin films [16], and 1300 F g^{-1} in nano-tubular structure [17].

Although RuO_2 has a substantially high specific capacitance, several problems have been observed such as short life time, performance deterioration under repeated cycles, and poor

performance at high charge/discharge rates [18-20]. The volume of RuO_2 in the form of granules or powder changes during charge/discharge because the lattice distance of 2.54 Å changes to 3.02 Å by the redox reaction, resulting in a substantial volumetric change during charge/discharge. Subsequently, the short life of the RuO_2-based supercapacitor was shown to incur a fatal weakness for wide utilization and a rapid deterioration of performance at high scan rates which limits the practical applications of RuO_2 as supercapacitor electrodes [21]. It has been reported that the specific capacitance of hydrous RuO_2 rapidly decreases by 42% with increasing scan rates from 2 mV s^{-1} (720 F g^{-1}) to 50 mV s^{-1} (300 F g^{-1}) [4].

A method to improve the cycling stability of hydrous RuO_2 and obtain preferable electrochemical performance may be the use of hybrid technology by adding various carbon-based materials (activated carbon, carbon nanotubes, and graphene)to binder materials, mostly polymers [22-25]. For example, Sonia et al. [26] successfully prepared a hybrid supercapacitor electrode (activated carbon/carbon black/RuO_2) with a binder material (PTFE). However, the binder materials can increase the electrical resistance of the electrode and decrease the active surface area of the metal oxide. In addition, the binder interface is often damaged by the repeated charge/discharge process due to the volumetric expansion/contraction of RuO_2 [27,28]. Subsequently, binder-free metal oxide/carbon electrodes have been investigated, such as in chemical vapor deposition (CVD) and reactive sputtering techniques [29-35]. Recently, the binder-free thin layer electrode (~100 nm) by CVD could reach as high as 1652 F g^{-1} [36]. However, it should be mentioned that the layer formed by CVD is very thin, i.e., in a nanometer range, and thus the total amount of energy per unit electrode area should be very low in the supercapacitor module [37]. For commercialization, the supercapacitor electrode should be sufficiently thick for storing a considerable amount of energy.

In this study, a compressed powder-type electrode was tested, where the RuO_2/carbon powder was compressed by the external pressure without using binders. As a carbon electrode source, activated carbon has been chosen to reduce the cost drawback of hydrous RuO_2 and to provide a high surface area, resulting in a high electric double layer capacitance [38,39]. In addition, carbon black was added as a conductive agent for enhancing the conductivity of our hybrid electrodes [40]. Since the binder was not used in this novel system, the internal electrical resistance was substantially lowered, resulting in high power density, high energy density, and fast charge/discharge speed. More importantly, since the mechanical compression was maintained on the RuO_2/carbon powders during the charge/discharge process, the electrode failure caused by the volumetric change of the RuO_2 particles was successfully avoided to give a substantially enhanced life and performance to the pseudocapacitor.

Results and discussion

Figure 1 schematically compares the typical binder-containing and binder-free systems. In a typical binder-containing system (Figure 1A), which is commonly used in RuO_2 supercapacitor systems, the binder polymer can cover the active surfaces of RuO_2 and carbon powders, partially insulating the particle-to-particle and/or particle-to-current collector interfaces, which usually causes poor contact among the active materials. The binder materials could interrupt the facile transport of both protons and electrons in the supercapacitors. In addition, the binder interface can be easily broken by the repeated volume changes accompanied by the charge/discharge processes of hydrous RuO_2 materials. However, for the binder-free system shown in Figure 1B, the particle contact can be maintained by the external pressure by using devices such as lead springs or a compressible elastomer enclosed in a cell container. This provides excellent and direct contact between particles, which may

allow substantially enhanced energy storage performance in terms of capacitance and life. The improved contact among the active particulate materials may reduce the internal resistance of the electrode, resulting in high specific capacitance and high power density. Furthermore, as discussed earlier, the hydrous RuO_2 powders repeatedly expand and shrink during charge and discharge, respectively, which often destroys the binder-RuO_2 interface, resulting in poor long-term durability. In our binder-free system, however, an excellent contact is maintained during the volumetric shrinkage/expansion of hydrous RuO_2 powders, which could substantially improve the life of the hydrous RuO_2-based supercapacitors.

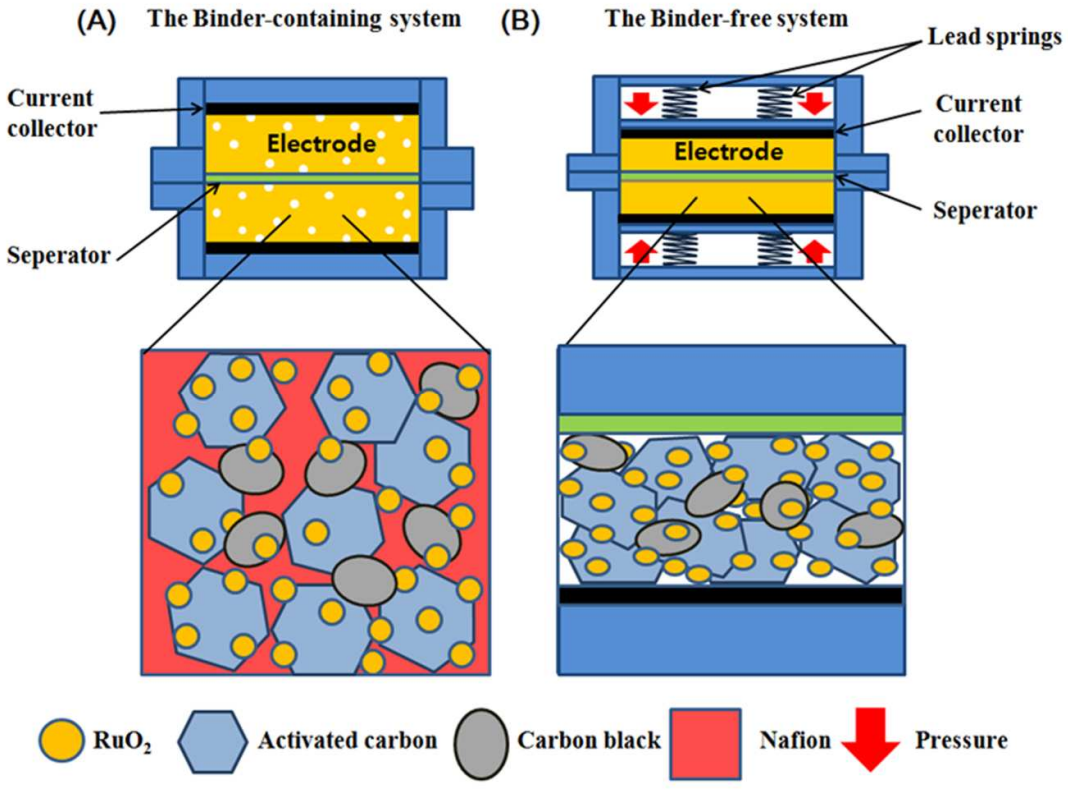

Figure 1. Schematic of the pseudocapacitor cell for (A) the binder-containing and (B) the binder-free systems.

The two supercapacitor cells, binder-free and binder-containing systems, are compared in Figure 2 and Table 1. Figure 2A shows a comparison of the galvanostatic charge/discharge

behavior between the binder-containing and binder-free systems. In the binder-free system, as schematically seen in Figure 2B, unless otherwise stated, the external pressure was fixed as 4.83 $kg_f\,cm^{-2}$. For both systems, quasi-linear and symmetric curves can be seen, which is a typical feature of RuO_2supercapacitors [15,18].

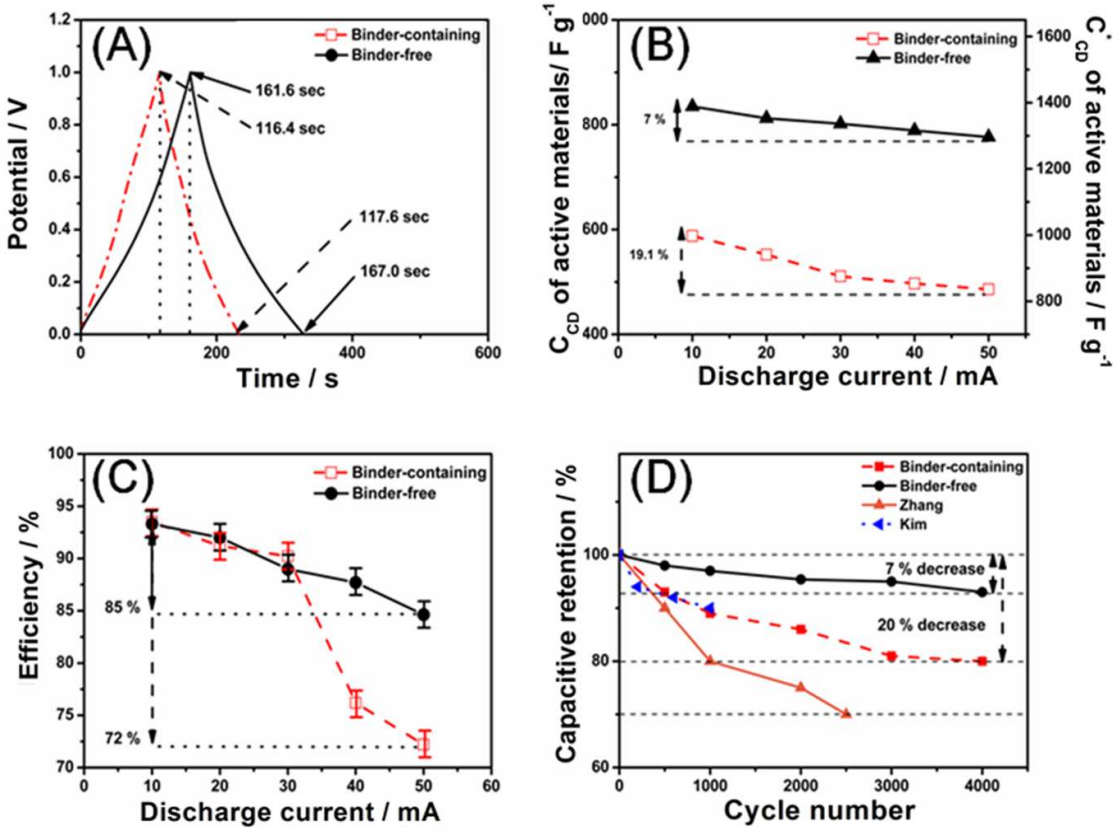

Figure 2. Supercapacitor performance comparing binder-containing and binder-free cell systems (60 wt% of RuO_2): (A) Galvanostatic charge/discharge (10 mA), (B) specific capacitances based on the weight of active electrode material (C_{CD}) and RuO_2 weight (C^*_{CD}), (C) electrochemical efficiency, and (D) capacitance retention plotted as a function of galvanostatic cycles ($0 < V < 1$), where the reference capacitance values at 100% are 835 and 588 Fg^{-1} for our binder-free system and binder-containing systems, respectively (10 mAs^{-1}). Herein, two values reported in the literature [15,22] are included for comparison in (D) with data re-plotted capacitive retention using the 100% reference values of 357 and 312 F g^{-1}.

Table 1. Total charge/discharge capacitance (C_{CD}) of the binder-containing and the binder-free systems at different discharge currents from 10 to 50 mA.

Samples		Discharge current (mA)				
		10	20	30	40	50
Binder-containing	Charge/Discharge time (t)	126.5/117.6	61.5/56.0	38.2/34.5	31.9/24.7	26.4/19.0
	Capacitance ($F\ g^{-1}$)	588	562	517.4	493	475.7
	Efficiency (%)	93	91.4	90.2	77.3	72
Binder-free	Charge/Discharge time (t)	179.6/167	88.9/81.2	59.7/53.9	51.2/39.6	43.1/31.1
	Capacitance ($F\ g^{-1}$)	835	8.2	808	791.4	776.6
	Efficiency (%)	93	91.8	89.2	87	85.1

Based on the charge/discharge curves, the specific capacitance (C_{CD}) by the galvanostatic charge/discharge measurement can be calculated using the following equation [41,42]:

$$C_{CD} = 2(I \times \Delta t)/(m \times \Delta V) \quad (1)$$

where I is the discharge current, m is the mass of active materials(total amount of activated carbon, carbon black, and hydrous RuO_2), and Δt is the time required for discharging the pseudocapacitor during the voltage drop of ΔV. The specific capacitance of the RuO_2(C^*_{CD}) was recalculated using the masses of RuO_2 and the active material, viz: $C^*_{CD} = C_{CD} / 0.6$ (as an electrode contained 60 wt% of RuO_2).

The maximum specific capacitance value is 588 Fg^{-1} for the binder-containing system, which is similar to the value of typical RuO_2/carbon/binder systems, e.g., 595 F g^{-1} reported in the literature [43,44]. This observed value indicates that a difficulty might arise with the ability of the electric charges to occupy the available sites at the interface between active materials due to the interference of the binder material [45]. However, the maximum

capacitance of 835 F g^{-1}can be obtained at 10 mA in the binder-free system, which is much higher than that of the 588 F g^{-1}. The significant enhancement in specific capacitance is due to the positive synergetic effect, whereby the compression of active materials can effectively reduce the interfacial resistances among these materials, and consequently provide an available electrochemically active surface area for exploiting the full advantages of hydrous RuO_2 pseudocapacitance and carbon-based double layered capacitance [26,46].

Figure 2B shows the specific capacitances of binder-containing and binder-free systems plotted as a function of different discharge currents ranging from 10 mA to 50 mA. As the discharge current is increased, both systems exhibit decreasing capacitances as a typical behavior of pseudo-capacitance materials [47]. However, our binder-free system shows much smaller decrement of capacitance at 7%, which should be compared with the binder-containing system at 19.1%. It should also be mentioned that C_{CD} (or C^*_{CD}) of the binder-free system ranges from 776.5 to 835 F g^{-1} (1294.3 to 1391.7 F g^{-1}), which is much higher than the range in the binder-containing system of from 475.7 to 588 F g^{-1} (792.8 to 980.0 F g^{-1}). It is clearly seen that the specific capacitance of our binder-free system shows much improved performance of specific capacitance and its retention in high discharge rates seemingly due to the enhanced packaging efficiencies and facile transport of ions in the redox reactions and Faradaic transfer.

The electrochemical efficiency may be defined as the ratio of charge/discharge areas ($A_{Discharge}$ /A_{Charge}) as shown in Figure 2C. As can be seen, the efficiency decreases with increasing current densities, as for most supercapacitors. For example, comparing the 10 and 50 mA current densities, the efficiency of the binder-containing system sharply decreases from 93% to 72%, while that of the binder-free system decreases from 93% to 85%. Therefore, this result shows that debonding failure at the interface between the hydrous RuO_2

powders and polymer binders is caused by the repeated charge/discharges in the binder-containing system. However, in the binder-free system, the capacitive stability can be achieved through the efficiently compressed RuO_2/carbon powder materials without the volumetric change of the electrode. We believe that this could then give substantially improved power densities and rate-dependent capacitances of RuO_2 systems.

In Figure 2D, the capacitive retention of our supercapacitor system is evaluated up to 4000 galvanostatic cycles in this study. After 4,000 cycles, the binder-free system supercapacitor retains 93% of its initial specific capacitance, which should be compared with 80% of the binder-containing system. This capacitance loss after 4,000 cycles can probably be ascribed to the saturation and reduction of protons in the electrolyte-electrode interface during cycling [48]. However, these results prove that the binder-free system has an excellent cycle stability and very high degree of reversibility in the repetitive charge/discharge cycling. As also compared in Figure 2D, two literature values reproduced from two references [19,25] show much faster deterioration of capacitance than our binder-free system. This excellent cycling performance of the developed binder-free RuO_2/carbon powder-type electrode can be attributed to the fact that the RuO_2 particles are effectively compressed by the external pressure without binders. In addition, the binder-interface failure, which is caused by the volumetric fatigue of RuO_2 particles under a repeated charge/discharge process, can be avoided by our binder-free system of RuO_2 supercapacitor. Furthermore, the applied pressure can also improve the pore-filling efficiency in the supercapacitor [49] that the high pore-filling efficiency by the binder-free system may be the reason for the improved stability.

Figure 3 shows the cyclic voltammetry (CV) measurements of the RuO_2/carbon electrodes (60 wt% of RuO_2), comparing the binder-containing and the binder-free systems. As seen in Figures 3A and 3B, the current density of the binder-free system exhibits higher

current values than that of the binder-containing system at the same voltage scan rates, indicating that the capacitance of the binder-free system would be higher than the binder-containing system. In addition, Figures 3A and 3Bshow redox peaks, which suggest pseudo-capacitance behavior of the RuO_2 electrode [41,42]. While a single-broad redox peak appears for the binder-free system, it is interesting to note that two redox peaks are observed for the binder-containing system. These peaks indicate the existence of a redox process due to the presence of carboxyl, carbonyl, and phenol groups bound to the surface of the activated carbon and carbon black [50].

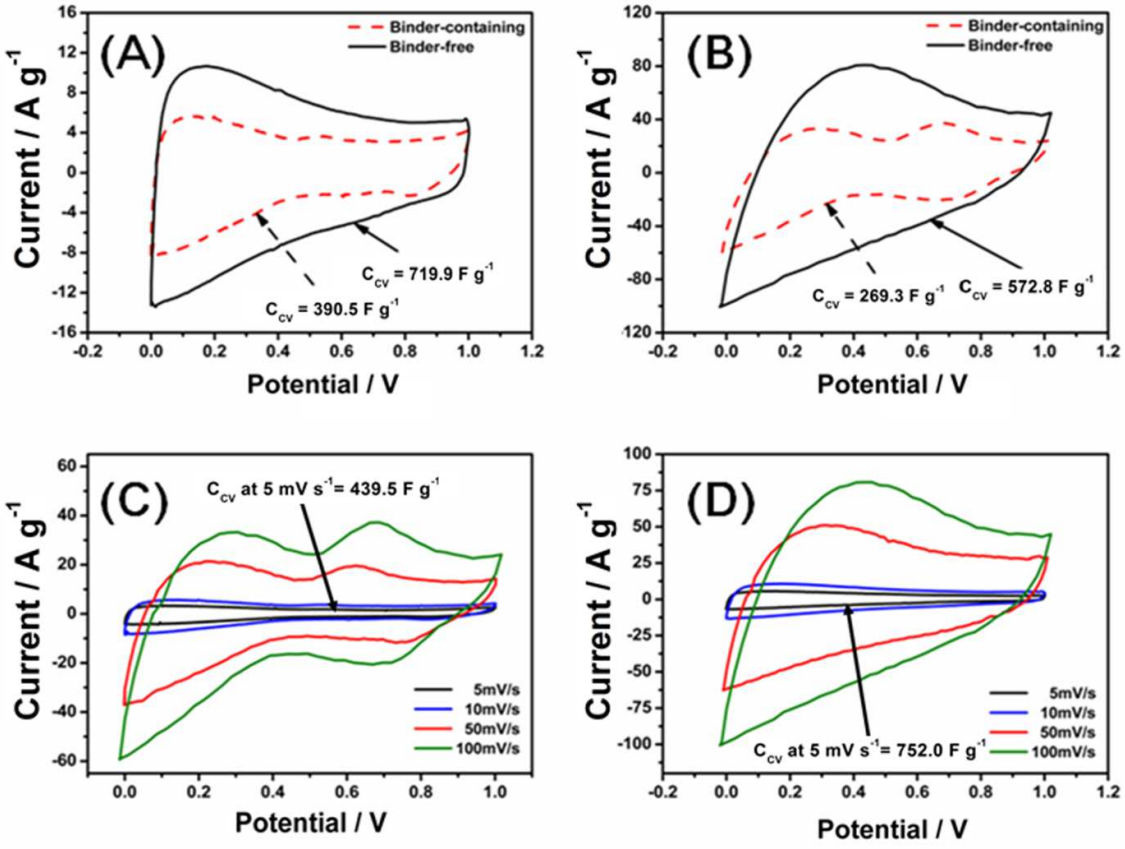

Figure 3. Cyclic voltammograms of the binder-containing and the binder-free systems at voltage scan rate of 10 mVs^{-1} (A) and 100 mVs^{-1} (B). Effect of voltage scan rates for the binder-containing (C) and the binder-free (D) systems.

The specific capacitance obtained from the CV results (C_{cv}) can be calculated using the following equation [20]:

$$C_{CV} = 2I/(m \times dV/dt) \quad (2)$$

where dV/dt is the potential sweep rate. As indicated in Figures 3A and 3B, the evaluated specific capacitances calculated using equation 2 are 390.5 and 719.9 F g^{-1} for the binder-containing and the binder-free systems, respectively, at the voltage scan rate of 10 mV s^{-1}. The specific capacitances at a high scan rate of 100 mV s^{-1} are 269.3 and 572.8 F g^{-1} for the binder-containing and the binder-free systems, respectively. These C_{CV} values of the binder-free system are almost twice those of the binder-containing system at both voltage scan rates. These results demonstrate that the binder-free system gives excellent energy-storage efficiency, exerting the utmost intrinsic capability of RuO_2 materials.

The CVs at different scan rates of 5, 10, 50, and 100 mVs^{-1} are shown in Figures 3C and 3D for the binder-containing and binder-free systems. It can be seen that the CV area of both systems increases with increasing voltage scan rates, highlighting a clear dependence of current density on scan rate [51]. In addition, all CV curves have redox peaks and exhibit a quasi-symmetric shape, indicating that the charge/discharge process of active materials is mainly carried out by the pseudocapacitive characteristics of RuO_2 materials over all the scan rates [4,52]. Two redox peaks can be seen over the voltage scan rate of 5 mVs^{-1} in the binder-containing system, which may be attributed to the fact that the binder materials interrupt the intimate interaction between the active materials and the electrolyte. However, for the binder-free system, only a single broad redox peak is seen over all the scan rates, seemingly due to the intact electrochemical reactions of the RuO_2/carbon without interruption by binder materials. The maximum specific capacitance values are 752.05 F g^{-1} for the binder-free

system and 439.5 F g^{-1} for the binder-containing system at 5 mV s^{-1}, corresponding to 71% enhancement with the binder-free system. This may be attributed the fact that the RuO_2 surface is completely exposed to the electrolyte since the binder material is not used. In addition, it should be noted that the RuO_2 and carbon particles are forced to be in contact during the charge/discharge process due to the applied external pressure as designed in this study.

Figure 4 and Table 2 compare the total specific capacitance (C_{CV}), which is based on the total mass of the electrode, and the specific capacitance of RuO_2 (C^*_{CV}), which is based on the mass of RuO_2, plotted as a function of scan rates ranging from 5 mV s^{-1} to 100 mV s^{-1}. Comparing the scan rates of 5 and 100 mV s^{-1}, C_{CV} for the binder-containing system decreases sharply by 38.7%. However, only a reduction of 23.9% in the C_{CV} and C^*_{CV} values is observed for the binder-free system. In the binder-free system, the maximum C^*_{CV} value reaches 1253 F (g of RuO_2) $^{-1}$ at a scan rate of 5 mVs^{-1}. Even at a high scan rate of 100 mV s^{-1}, the C^*_{CV} value is 954.6 F(g of RuO_2) $^{-1}$. These values are comparable to the highest values of C_{Ru} reported by C.C. Hu et al. (690 F g^{-1} measured at 25 mV s^{-1}) [53] and I.H. Kim et al. (1170 F g^{-1} measured at 10 mV s^{-1}) [54], both of which were measured as a thin film (0.2 ~ 0.3 mg cm^{-2}), i.e., seemingly the maximum achievable capacitance of RuO_2. The C^*_{CV} value in the binder-containing system is 813.8 F (g of RuO_2) $^{-1}$ at a scan rate of 5 mVs^{-1}, which is not as high as the binder-free system but similar to the published values for most binder-containing RuO_2 systems [55]. This demonstrates that the binder-free system allows excellent charge/discharge capability, which has not been achieved in previous studies of the powder form of RuO_2 supercapacitor systems.

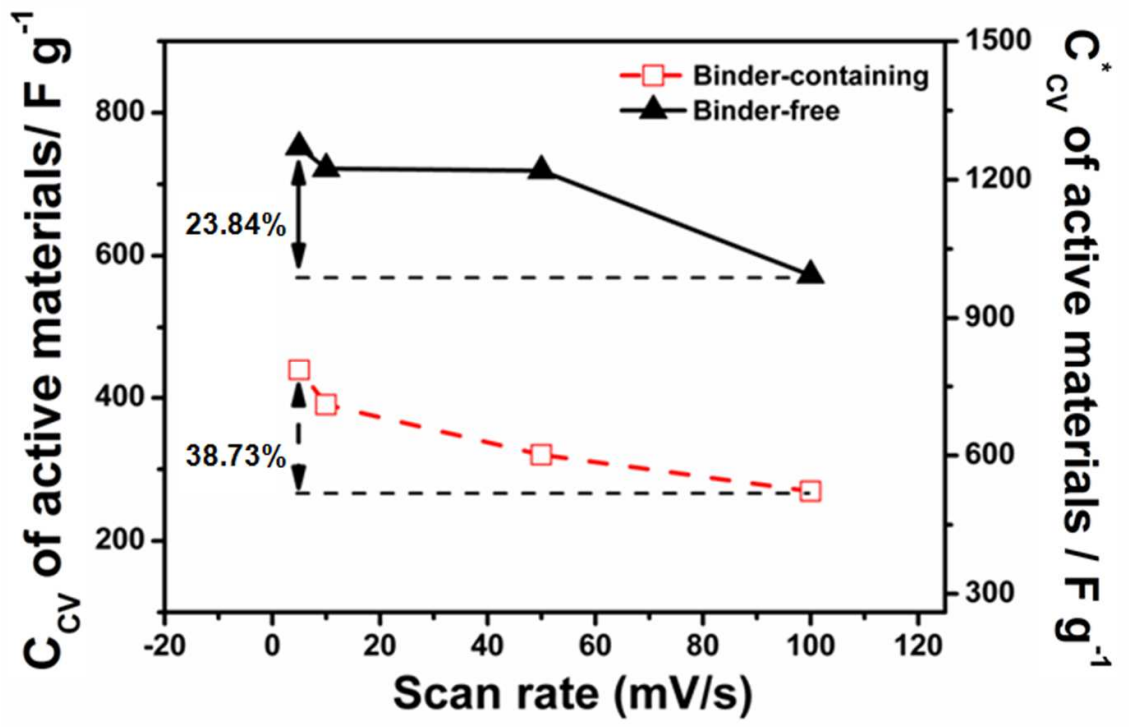

Figure 4. Specific capacitances based on the weight of total electrode materials and RuO_2 for the binder-containing and the binder-free systems as a function of scan rates.

Table 2. Specific capacitances of C_{CV} and $C^*_{CV}$for the binder-containing and the binder-free systems at different scan rates of 5, 10, 50, and 100 mVs^{-1}.

Samples		Specific capacitance (Fg^{-1})			
		5 mV s^{-1}	10 mV s^{-1}	50 mV s^{-1}	100 mV s^{-1}
The binder-containing system	C_{CV} F (g of active materials)$^{-1}$	439.5	390.52	320.34	269.32
	C^*_{CV} F (g of RuO_2)$^{-1}$	813.8	723.18	593.23	498.7
The binder-free system	C_{CV} F (g of active materials)$^{-1}$	752.05	719.9	718.96	572.8
	C^*_{CV} F (g of RuO_2)$^{-1}$	1253.4	1199.8	1198.2	954.6

Figure 5A shows the Nyquist plots, the real vs. the imaginary part of the complex impedance as represented by Re (Z) vs. Im (Z), respectively, of the binder-containing and binder-free systems measured in the frequency range between 0.01 Hz and 100 kHz. At high

frequencies (> 10 kHz), the cell behaves similar to a simple resistor, and these resistance values can be interpreted as bulk resistance [8]. This includes the electrolyte resistance (R_S) of the cell and the bulk resistance of the electrode, which may be derived from the intersection of the curves in the real axis (Im Z = 0). Since the same electrolyte was used (1M H_2SO_4), R_S becomes similar at 0.31 Ω and 0.37 Ω for the binder-containing and binder-free systems, respectively. In the high-to-medium frequency region (1 Hz to 10 kHz), semicircles can be observed in both systems, which correspond to a parallel combination of charge-transfer resistance (R_{ct}) and double layer capacitance (C_{DL}) [56,57]. The size of the semicircle of the binder-containing system is much larger than that of the binder-free system, indicating a poor electrochemical reaction at the electrode/electrolyte interface, seemingly because the binder materials are placed at the particle interface acting as an insulator [26]. On the other hand, the semicircle size of the binder-free system is relatively small. This can be associated with the good electronic conductivity among active materials such as activated carbon, carbon black, and hydrous ruthenium particles. Furthermore, another possible explanation could be the improved contact between the current collector and these active materials [58].

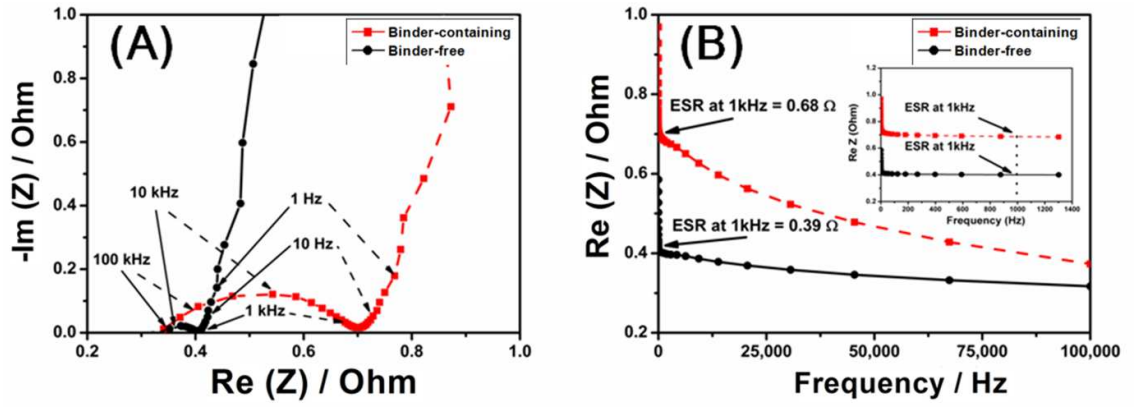

Figure 5. Nyquist plots of a comparison of the binder-containing and the binder-free systems (A) and its real part impedance (B) measured in the frequency range from 0.01 Hz to 100 kHz in 1 M H_2SO_4.

At frequencies between 1 Hz and 10 Hz, "the Warburg region" is related to the frequency dependence of ion diffusion on the electrode interface in the electrolyte [59]. The resistance value may be evaluated from the intersection of the Warburg line with the real axis. It can be seen that the resistance of the binder-free system is much smaller (0.415 Ω) than that of the binder-containing system (0.71 Ω). This also demonstrates that the contact between the active particulate materials and electrolytes is improved by the external pressure from the binder-free system. At lower frequencies (< 1 Hz), the Nyquist plot approaches a vertical line, giving the resistances of 4.5 Ω and 7.6 Ω for the binder-free and binder-containing systems, respectively. These results demonstrate that the internal cell resistance of the binder-free system has substantially reduced values.

Figure 5B shows the real part of impedance plotted as a function of frequency, which may be referred to as an equivalent series resistance (ESR) [8]. As can be seen, the ESR increases with decreasing frequency for both systems. It is clear that ESR values for the binder-free system are much lower than those of the binder-containing system. For example, the ESR of the binder-free system is 0.39 Ω at 1 kHz, which is lower than that of 0.68 Ω for the binder-containing system. This indicates that the binder-free system has a good electric conductivity due to the excellent electrical contact between the RuO_2, carbon materials, and current collector, due to the external pressure applied to the powders with no use of binder materials, as proposed in this study.

The specific energy (E_{CV}, Wh kg^{-1}) and specific power (P_{CV}, kW kg^{-1}) can be calculated by C_{CV}, using the following equation [60]:

$$E_{CV} = (C_{CV} \times \Delta t)/8 \quad (3)$$

$$P_{CV} = (C_{CV} \times V)/\Delta V \quad (4)$$

The specific energy density, E_{CV} (v), is shown in Figure 6A as a function of specific power density, P_{CV} (v), comparing the binder-containing and the binder-free systems. As can be seen in this Ragone plot, energy densities decrease with the scan rate. As previously mentioned, the energy density of RuO_2 usually decreases rapidly at high voltage scan rates, which has been pointed out as a drawback of RuO_2 materials, critically limiting the wide utilization of RuO_2materials for high-energy density supercapacitors. As seen in Figure 6A, the energy density of the binder-free system is maintained as 24.9 ~ 26.1 W h kg^{-1}at the scan rates of 5 ~ 50 mV s^{-1}. However, the energy density of the binder-containing system gradually decreases from 15.2 to 11.1 Wh kg^{-1} in the same scan rate region. More specifically comparing the energy densities at the voltage scan rate at 50 mV s^{-1}, the binder-free system shows the energy density at 24.9 Wh kg^{-1}, which is ca. 55.5% higher than that of the binder-containing system (11.1 Whkg^{-1}). Accordingly, the power density of the binder-free system can be much higher than the binder-containing system. For example, it reaches 16.1 and 7.2 kW kg^{-1} at 50 mV s^{-1} for the binder-free and the binder-containing systems, respectively, which corresponds to ca. a two-fold increment in the binder-free system.

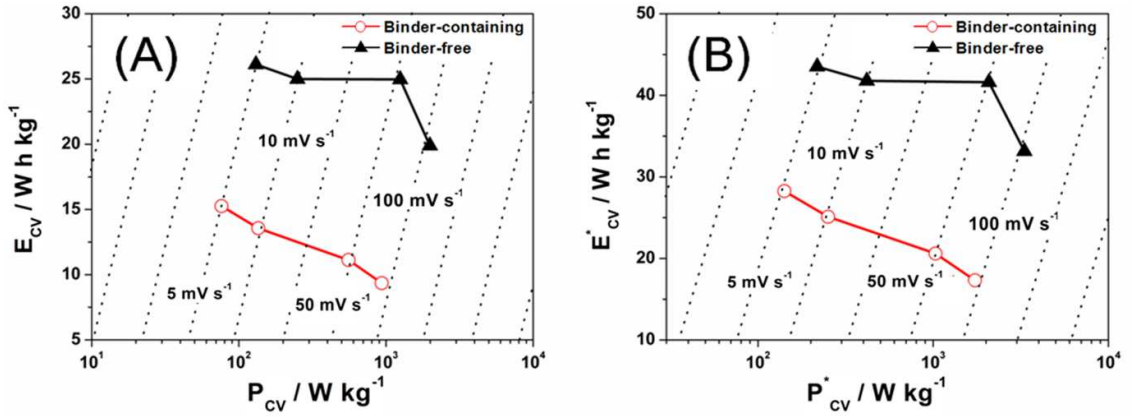

Figure 6. Ragone plots comparing the binder free and the binder-containing systems. (A) and (B) are based on the weight of total active materials C_{CV} and RuO_2 powder C^*_{CV}, respectively.

The Ragone plots evaluated on the basis of the pure RuO_2 weight, represented by E^*_{CV} vs.

P^*_{CV}, is shown in Figure 6B. It can be seen that E^*_{CV} and P^*_{CV} of the binder-free system reach 41.6 Wh kg^{-1} and 26.9 kW kg^{-1}, respectively, at 50 mV s^{-1}. In addition, the maximum specific energy and power densities reach as high as 43.5 Wh kg^{-1} (at 5 mV s^{-1}) and 42.9 kW kg^{-1} (at 100 mV s^{-1}), respectively, for the binder-free system. These values are collectively considered to be excellent compared with the values of RuO_2/carbon nano-composite systems in the reported literature; e.g., reported as 25 Wh kg^{-1} and 21 kW kg^{-1} [20], 18.8 Wh kg^{-1} and 96 kW kg^{-1} [61]. The pseudocapacitive reaction of RuO_2 usually takes place at the surface, and the surface exposure of the RuO_2 powder is thus important. In the binder-containing system, the binder material covers the RuO_2 powder surface, which seems to substantially reduce the energy storage capability. However, an excellent capacitive performance of the binder-free system can be obtained, which is probably ascribed to the decrease of ESR with good packaging efficiency due to the compressed powder system. Significantly, the binder-free system accelerates the charge transfer through the electric double layer, while the hydrous RuO_2 provides a more electrochemical active surface for fast and reversible Faradic reaction. In this sense, our binder-free system demonstrates that the electrochemical performance of the RuO_2 powder electrode can be greatly improved in terms of high energy and power densities, low ESR, response to scan rate, and long-term durability.

Experimental

Materials preparation

RuO_2/carbon pseudocapacitor electrodes were prepared by mixing activated carbon (DLC 150 Supra NORIT), carbon black (acetylene black ALFA AESAR), and hydrous RuO_2powders (Sigma Aldrich) at a ratio of 3 : 1: 6 for our “binder-free system”. For comparison, the same composition and weight of the electrode materials was mixed with

Nafion (50% concentration, Sigma Aldrich) as a binder material for a "binder-containing system". The solid content of Nafion was 10% of the total electrode weight. A small amount of 1M H_2SO_4 was added to prepare slurries for both systems. The mixtures were sonicated for 15 min at 30 ^oC.

Before the coating process, an appropriate amount of 1 M H_2SO_4 was added to the mixed active material pastes to optimize the viscosity. The amount of additional 1 M H_2SO_4 was varied from 10 to 20 times higher than the active materials. Although not included here, we obtained an optimizing weight proportion of the active material and H_2SO_4. After preparing the active pastes, the hybrid capacitor electrode was fabricated by coating the RuO_2/carbon pastes onto a graphite film. As mentioned above, the slurry consisted of active materials with 1 M H_2SO_4 (which can oxidize the metallic substrate) that we chose as a highly conductive graphite film as an alternative current collector. In addition, graphite film can be a cost effective and lightweight substrate for the conventional application. The thickness of both the cathodic and anodic electrodes was adjusted at around 150 ± 10 μm by using a doctor blade. Although we used a doctor blade to control the thickness of the electrodes (fixed 150 μm), because the paste of active materials contains a high amount of 1 M H_2SO_4, we could expect that the real height of electrodes can be measured near 80 μm after eliminating the H_2SO_4 by calculating the volume and the proportion of active materials. In addition, when we fabricated the binder-containing pseudocapacitor, the mass loading of active materials was carefully calculated as 4 mg, without including the mass of binder materials. Furthermore, since the proportion of the binder material was only 5 wt% and its density is known to be 0.874 g cm^{-3}, we concluded that the height difference between the binder-free and the binder-containing electrode could be negligible. After coating the RuO_2/carbon pastes onto a graphite film, to obtain reliable capacitive results, the mass of the RuO_2/carbon electrode was carefully

measured after 30 minutes drying at 90 ^{o}C using a convection oven. The total weight of the RuO_2/carbon electrode in both binder-free and binder-containing systems was calculated as 4 mg without considering the mass of H_2SO_4 and binder material.

For evaluation of the cell performance similar to the actual capacitors, the pseudocapacitor cells were fabricated by sandwiching the two symmetrical RuO_2/carbon electrodes in disk shapes (diameter of 20 mm). A separator (TF4035 MKK) was placed between the symmetrical RuO_2/carbon electrodes and 1 M H_2SO_4 was used as an electrolyte. As shown in Figure 7, the RuO_2/carbon powder sample was placed between the compression metal tools and the I-V responses were monitored *in-situ* while maintaining a constant pressure at 4.83 $kg_f cm^{-2}$.

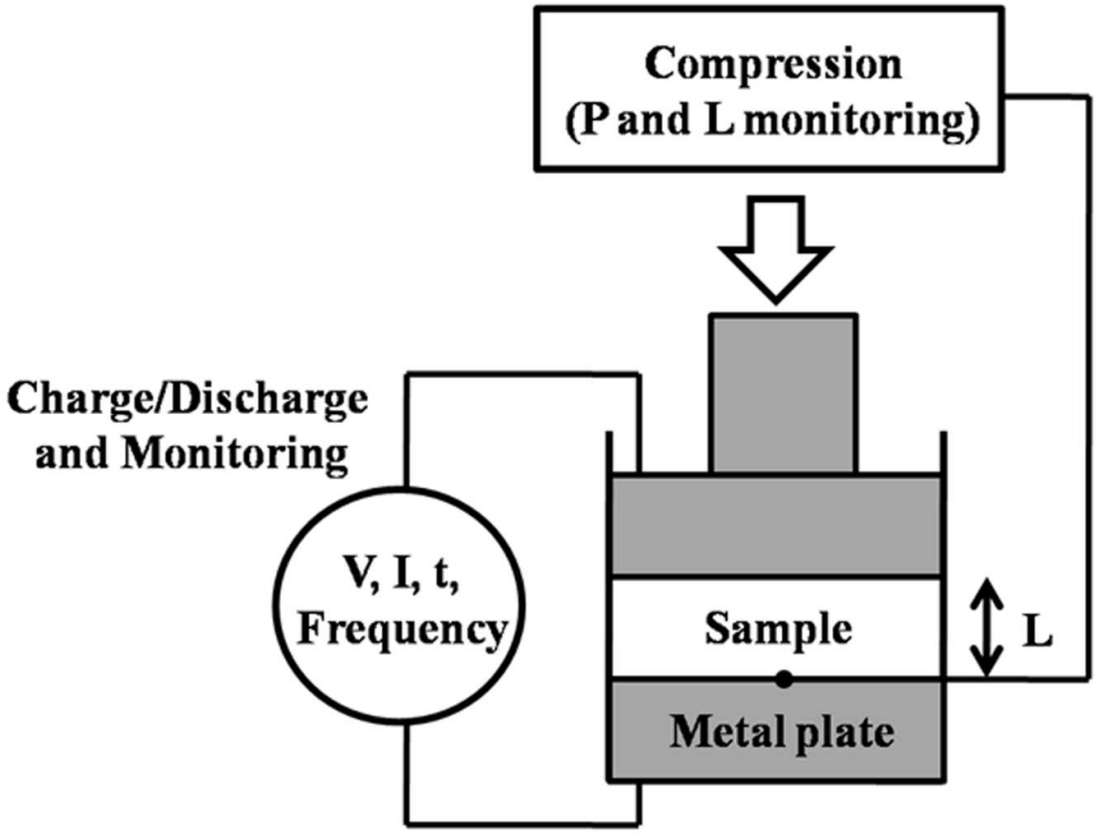

Figure 7. Schematic of the binder-free system and its experimental setup, exhibiting the RuO_2/carbon powder sample externally compressed using a universal testing machine.

Voltage (V), current (I), pressure (P), and length (L) were monitored as a function of time (t).

Characterization

The pseudocapacitor cells were characterized for both binder-containing and binder-free systems. Electrochemical characterization studies were carried out using a battery cycler (WBCS 5000, Won-A Tech). The cyclic voltammetry (CV) tests for both systems were measured at various scan rates of 5, 10, 50, and 100 mV s^{-1} in 1 M H_2SO_4. The galvanostatic charge/discharge tests were also carried out at various current densities (10 mA to 50 mA) between 0 and 1 V. The cycling behavior of RuO_2/carbon composite electrodes was measured at a current density of 10 mA for 4,000 cycles using galvanostatic charge/discharge techniques. Electrochemical impedance spectroscopy (SP-150 Biologic) was used for measuring the complex internal resistance values at frequencies ranging from 100 kHz to 0.01 Hz.

Conclusion

This work explored a novel technique of a compressed binder-free system. Electrochemical measurements in a stack assembly showed that the binder-free system gave specific capacitance up to 835 F g^{-1} (1391.7 F g^{-1} of RuO_2) of a discharge current at 10 mA in a 1.0 M H_2SO_4 aqueous electrolyte. This developed method also provided excellent cycle stability, with 93% of the initial specific capacitance retained after 4,000 cycles. In addition, only 23.9% reduction in the C_{CV} and C^*_{CV} values is observed for the binder-free system, even at a high scan rate of 100 mV s^{-1}. An excellent low ESR value of 0.39 Ω was also achieved for the binder-free system at the frequency of 1 kHz. Furthermore, the best performances of energy and power density were 24.9 Wh kg^{-1} and 16.1 kW kg^{-1}, respectively, at 50 mV s^{-1}. Based on

these excellent capacitive properties, the binder-free system provides a promising methodology for the development of high-power and high energy density pseudocapacitors.

Acknowledgements

This work was supported by the National Research Foundation of Korea (NRF) Grant funded by the Korean Government (NRF-2013R1A1A2064240). We also appreciate the project and equipment support from Gyeonggi Province through the GRRC program at Sungkyunkwan University.

Notes and References

[1] O. Herbert, *Chem. Rev*., 2012, **112**, 3356−3426

[2] E. Frackowiak, *Carbon*., 2001, **39**, 937-950.

[3] R. Kotz, M. Carlen, *Electrochim. Acta*., 2000, **45**, 2483-2498

[4] P. Simon, Y. Gogotsi, *Nat. Mater*., 2008, **7**, 845–854.

[5] Y. Zhang, H. Feng, X. B. Wu, L. Z. Wang, A. Q. Zhang, T. C.Xia, H. C. Dong, *Int. J. Hydrogen Energy*., 2009, **34**, 4889–4899.

[6] L. L. Zhang and X. S. Zhao, *Chem. Soc. Rev*., 2009, **38**, 2520-2531

[7] C. Liu, F. Li, L. P. Ma and H. M. Cheng, *Adv. Mater*., 2010, **22**, E28

[8] B. E. Conway, Electrochemical Supercapacitors: Scientific Fundamentals and Technological Applications; Kluwer Academic: New York., 1999

[9] S. Trasatti, In The Electrochemistry of Novel Materials; Lipkowski, J.; VCH Publishers: New York., 1994, 207

[10] B. K. Kim, V. Chabot, *Electrochim. Acta*. 2013, **109**, 370-380

[11] G. Yu, X. Xie, L. Pan, *Nano Energy*., 2013, **2**, 213-234

[12] C. D. Lokhande, D. P. Dubal, O. S. Joo, *Curr. Appl. Phys*., 2011, **11**, 255-270

[13] B. J. Lee, S. Sivakkumar, J. M. Ko, *J. Power Sources*., 2007, **168**, 546

[14] W. Deng, X. Ji, Q. Chen, *RSC. Advances*., 2011, **1**, 1171

[15] J. P. Zheng, P. J. Cygan, T. R. Jow, *J. Electrochem. Soc*., 1995, **142**, 2699-2703

[16] C. Sassoye, C. Laberty, H. L. Khanh, *Adv. Funct. Mater*., 2009, **19**, 1922

[17] C. C. Hu, K. H. Chang, M. C. Lin, Y. T. Wu, *Nano Lett*., 2006, **6**, 2690

[18] B.E. Conway, V. Birss, J. Wojtowicz, *J. Power Sources*., 1997, **66**, 1

[19] H. Kim, B. N. Popov, *J. Power Sources*., 2002, **104**, 52-61

[20] J. H. Jang, A. Kato, K. Machida, and K. Naoi, *J. Electrochem. Soc*., 2006, **153**, A321-

A328

[21] J. P. Zheng, *Solid. State. Lett*., 1999, **2**, 359-361

[22] X. Zhang, W. Shi, J. Zhu, W. Zhao, J. Ma, S. Mhaisalkar, T. L. Maria, Y. Yang, H. Zhang and H. H. Hng, *Nano Res*., 2010, **3**, 643

[23] A. Kumar, S. Ramaprabhu, *J. Phys. Chem. C*., 2011, **115**, 14006-14013

[24] J. Zhang, J. Jiang, *Energy Environ. Sci*., 2011, **4**, 4009-4015

[25] Y. F. Su, F. Wu, L. Y. Bao, *New Carbon Mater*., 2007, **22(1)**, 53-57

[26] S. Dsoke, X. Tian, C. Taubert, *J. Power Sources*., 2013, **238**, 422-429

[27] I. H. Kim, K. B. Kim, *J. Electrochem. Soc*., 2006, **153**, A383-389

[28] C. Chabanier, D. Guay, *J. Electroanal. Chem.*, 2004, **570**, 13-27

[29] R. Shi, L. Jiang, C. Pan, *Soft. Nanosci. Lett*., 2011, **1**, 11-15

[30] W. Dmowski, T. Egami, K. E. Swider, *J. Phys. Chem. B*. 2002, **106**, 12677

[31] K. H. Chang, C. C. Hu, C. Y. Chou, *Chem. Mater*., 2007, **19**, 2112

[32] Z. Niu, W. Zhou, J. Chen, G. Feng, H. Li, W. Ma, J. Li, *Energy Environ Sci*., 2011, **4**, 1440-1446

[33] W. Ma, L. Song, R. Yang, T. H. Zhang, Y. C. Chao, L. F. Sun, *Nano Lett*., 2007, **7**, 2307-2311

[34] R. Shah, X. F. Zhang, *Nanotechnology*. 2009, **20**, 395202

[35] C. Du, N. Pan, *Nanotechnology*., 2006, **17**, 5314-5318

[36] T. F. Hsieh, C. C. Chuang, W. J. Chen, *Carbon*., 2012, **50**, 1740-1747

[37] J. Zhang, J. Ma, L. L. Zhang, *J. Phys. Chem. C.*, 2010, **114**, 13608-13613

[38] C. Merino, P. Soto, *Carbon*., 2005, **43**, 551-557

[39] D. Y. Qu, H. Shi, *J. Power Sources.*, 1998, **74**, 99-107

[40] G. Salita, A. Soffer, *J. Electrochem. Soc*., 2000, **147**, 2486-2493

[41] M.D. Stoller, R. S. Ruoff, *Energy Environ. Sci*., 2010, **3**, 1294

[42] D. Hulicova-Jurcakova, A. M. Puziy, O.I. Poddubnaya, G. Q. Lu, *J. Am. Chem. Soc*., 2009, **131**, 5026

[43] Y. Chen, X. Zhang, P. Yu, *J. Power Sources*., 2010, **195**, 3013-3035

[44] R. R. Bi, X. L. Wu, F. F. Cao, *J. Phys. Chem. C*., 2010, **114**, 2448-2451

[45] D. P. Dubal, G. S. Gund, R. Holze, *Electrochim. Acta*., 2013, **103**, 103-109

[46] B. Marinho, M. Ghislandi, *Powder Technol*., 2012, **221**, 351-358

[47] J. P. Zheng, T. R. Jow, *J. Power Sources*., 1996, 62, 155-159

[48] L. Deng, J. Wang, G. Zhu, *J. Power Sources*., 2014, **248**, 407-415

[49] C. Masarapu et al, *Adv. Energy Mater.* 2012, **2**, 546-552

[50] Y. T. Kim, T. Mitani, *J. Power Sources*., 2006, **158**, 1517-1522

[51] D. P. Dubal, S. V. Patil, A. D. Jagadale, *J. Alloy. Compd*., 2011, **509**, 8183

[52] M. Xu, L. Kong, W. Zhou and H. Li, *J. Phys. Chem. C*., 2007, **111**, 19141

[53] C. C. Hu, C. C. Wang, K. H. Chang, *Electrochim. Acta*., 2007, **52**, 2691.

[54] I. H. Kim, J.-H. Kim, Y. H. Lee, K. B. Kim, *J. Electrochem. Soc*., 2005, **152**, A2170.

[55] Q. Wu, Y. Xu, Z. Yao, A. Liu and G. Shi, *ACS Nano*., 2010, **4**, 1963

[56] P.L. Taberna, P. Simon, E. Flahaut, *J. Power Sources*., 2005, **139**, 371-378

[57] A. Di Fabio, A. Giorgi, M. Mastragostino, F. Soavi, *J. Electrochem. Soc*., 2001, **148**, A845-850

[58] C. Portet, P. L. Taberna, P. Simon, *Electrochim. Acta*., 2004, **49**, 905.

[59] V.S. Bagotsky, Fundamentals of Electrochemistry 2nd edition; Wiley: NewYork, 2005

[60] Z. S. Wu, D. W. Wang, W. Ren, J. Zhao, *Adv. Func. Mater*., 2010, **20**, 3595

[61]P.Chen, H. Chen, J. Qiu, C. Zhou, *Nano Res*., 2010, **3**, 594-604